Pergamon

NanoStructured Materials, Vol. 5, No. 6, pp. 679-688, 1995
Elsevier Science Ltd

0965-9773/95 $9.50 + .00

0965-9773(95)00277-4

PHASE STABILITY IN NANOSTRUCTURED AND COARSE GRAINED ZIRCONIA AT HIGH PRESSURES

M. Winterer[1], R. Nitsche[1], S.A.T. Redfern[2], W.W. Schmahl[1*], and H. Hahn[1]

[1]Materials Science Department, Technical University Darmstadt, Germany
[2]Department of Earth Sciences, Cambridge University, United Kingdom
*now at: Department of Mineralogy, Tübingen University, Germany

(Accepted June 1995)

Abstract *— Zirconia powders with grain sizes from the nanometer (5 - 30 nm) to the micrometer (~1 μm) regime were investigated by in-situ high-pressure X-ray diffraction at pressures up to 14 GPa. In micrometer sized ZrO_2, a broad transition is observed at increasing pressure from the monoclinic to the orthorhombic polymorph. This first-order phase transition is, therefore, concluded to be martensitic in character. In the nanosized material, a metastable tetragonal polymorph exists and the stabilization is interpreted as a result of the surface stress of the nanocrystalline grains. An effective internal pressure in the particles above 2.5 GPa is estimated. The critical particle radius for the stabilization of the metastable phase in nanosized ZrO_2 is calculated to be 4-6 nm.*

INTRODUCTION

Coexistence of different polymorphs including metastable phases is a frequent characteristic feature of nanocrystalline (n-) oxide powders, *e.g.*, in ZrO_2 (1-4), Y_2O_3 (5,6), and Fe_2O_3(7). It has been observed that synthesis techniques and processing parameters influence the volume fraction of coexisting polymorphs. In particular, metastable phases may be stabilized by reducing the particle size into the nanometer regime. This stabilization is not only interesting as a finite size effect but also useful for controlling desireable properties such as superplasticity, as well as improving processing (*e.g.*, sintering) and enabling the production of new materials from nanometer sized particles.

In nanostructured zirconia particles two polymorphs have been identified at ambient conditions (1). One polymorph has monoclinic symmetry ($P2_1/c$) and is the stable phase in coarse grained material (of the order of μm) at ambient temperature and pressure. The second polymorph is tetragonal ($P4_2/nmc$) as determined by Rietveld profile analysis (4,8). The tetragonal phase is the stable high-temperature polymorph of coarse-grained zirconia and may be stabilized down to ambient conditions by impurities such as Ca^{2+} or Y^{3+}. For pure zirconia at ambient conditions the tetragonal phase is unique to nanocrystalline samples. The orthorhombic polymorphs (Pbca, Pbcm, $Pbc2_1$) are considered to be the stable high pressure phases in conventional ZrO_2 (9). The

second polymorph in the nanosized material is only metastable, because slight milling of the n-ZrO_2 powder in a mortar completely converted tetragonal n-ZrO_2 to monoclinic ZrO_2 without increasing the particle size.

It is long known that such size effects exist for ZrO_2. Garvie found experimentally a critical crystallite diameter of about 30 nm for the formation of the tetragonal phase (2). The monoclinic to tetragonal phase transition of ZrO_2 at high temperature is martensitic (13,14). Therefore, similar behavior is expected for the phase transition with increasing high pressure. Martensitic phase transitions are athermal and exhibit a broad first-order transition interval characterized by metastable phase coexistence because of large strains in the sample. Strains are often observable from the broadening of diffraction lines. If, however, the particle size is below the domain size of the martensitic phase, we expect a different behavior (narrow phase transition, shift of critical pressure). Here, we present first results of *in-situ* high-pressure diffraction of nanometer and micrometer sized ZrO_2 particles, and explore the nature of high-pressure transformations in both types of samples.

The stability of the tetragonal phase in small particles can be interpreted in terms of an increased effective internal pressure, which, in analogy with the Laplace equation for liquid drops, is inversely proportional to the particle radius:

$$\Delta p = \frac{2\sigma}{r} \qquad [1]$$

Here σ is the surface tension, r is the particle radius and Δp is the difference between external and internal pressure. In solids, surface tension σ has to be replaced by the surface stress f (10), which in the isotropic case is given by:

$$f = \sigma + \frac{d\sigma}{d\varepsilon} \qquad [2]$$

with ε is the strain. In solids, internal hydrostatic pressure is due to the surface stress which is of the order of the surface energy (11). For spherical, isotropic particles an equation analogous to [1] may be written by substituting σ by the surface stress f. Since the surface stress can both be positive and negative, it is possible to have compressive and expansive internal pressure in small solid particles. Similar effects have been found in thin solid films (12).

EXPERIMENTAL

(a) Sample Preparation

Pure ZrO_2 powders with two different grain sizes were used: commercial ZrO_2 with a grain size of approximately 1 μm, and n-ZrO_2 powder with a mean diameter of 11 nm, prepared by the gas condensation method (15). Zirconium suboxide was evaporated in an UHV-chamber, clusters formed in a low pressure (1Pa) He atmosphere and condensed on a cold finger cooled by liquid nitrogen. Particles were then oxidized by the inlet of pure molecular oxygen into the chamber

forming n-ZrO_2. The grain size of the nanostructured ZrO_2 was determined as 5 to 30 nm by dark field imaging using a Philips CM20 High Resolution Transmission Electron Microscope with a point to point resolution of 0.19 nm. Coarse grained ZrO_2 powder was obtained from AUER-REMY (Hamburg/Germany). The phase content was determined by X-ray diffraction using a STOE diffractometer operating in transmission mode.

(b) High-Pressure Diffraction

High-pressure experiments were carried out up to 14 GPa using both angle-dispersive and energy-dispersive X-ray powder diffraction at stations 9.1 and 9.7, respectively, of the wiggler beam line of the Daresbury synchrotron radiation source. In both cases experiments were performed at room temperature, using static loading in the diamond anvil cell and a non-dried mixture of methanol:ethanol = 4:1 as the pressure transmitting medium. Preindented inconel gaskets with 100 μm holes were used.

Angle-dispersive diffraction patterns were recorded at station 9.1 using an image plate system with X-rays of wavelength 0.04651 nm selected from a channel-cut $Si_{(111)}$ monochromator. Image plate data were converted to diffractograms with the program PLATYPUS (16). Pressure was measured *in-situ* by the shift of the ruby R fluorescence lines (17). Loading conditions remained hydrostatic throughout the experiment as indicated by the narrow width of the fluorescence lines.

High pressure powder diffraction patterns were also measured at station 9.7 using energy dispersive diffraction. White radiation, collimated by a 150 μm pinhole, was diffracted at $2\Theta = 5.96249°$ (as determined from the diffraction pattern of NBS silicon standard 640b) and further collimated along 500 mm long molybdenum receiving flats, shimmed apart by 100 μm. Spectra were recorded between 5 keV and 120 keV using a lithium drifted Ge detector with a resolution varying between 149 eV at 5.9 keV and 468 eV at 122 keV. Pressure was determined using the measured cell parameters of NaCl, which was mixed with the sample to act as an internal pressure calibrant, employing the equation of state of Decker (18). The estimated uncertainty in the pressure readings is ± 2%. ZrO_2 and NaCl diffraction peaks were measured by Gaussian peak fitting of the diffracted intensity.

RESULTS AND DISCUSSION

(a) Coarse-grained ZrO_2

The diffraction pattern at ambient pressure indicates the presence of monoclinic zirconia only (Figure 1). As can be seen from Figure 1 (data were fitted with a gaussian) an additional diffraction peak appears at pressures above 2.5 GPa. We assign this peak to the formation of a high pressure phase. With the present resolution we cannot distinguish between the tetragonal ZrO_2 and its slightly distorted orthorhombic variant. Both polymorphs have a higher density ($\rho_{(tet)} = 5.94$ g/cm^3 and $\rho_{(orth)} = 6.20$ g/cm^3) at ambient conditions than the monoclinic phase ($\rho_{(mon)} = 5.82$ g/cm^3) which would favor their formation at high pressures. Peak intensities corresponding to the proportion of monoclinic phase decrease with increasing pressure while the $(111)_{orth}$ peak (d = 2.9 Å) increases in intensity. Energy-dispersive data of ZrO_2 partially overlap with the data of the NaCl standard. Therefore, only the angle-dispersive measurements were analyzed quantitatively.

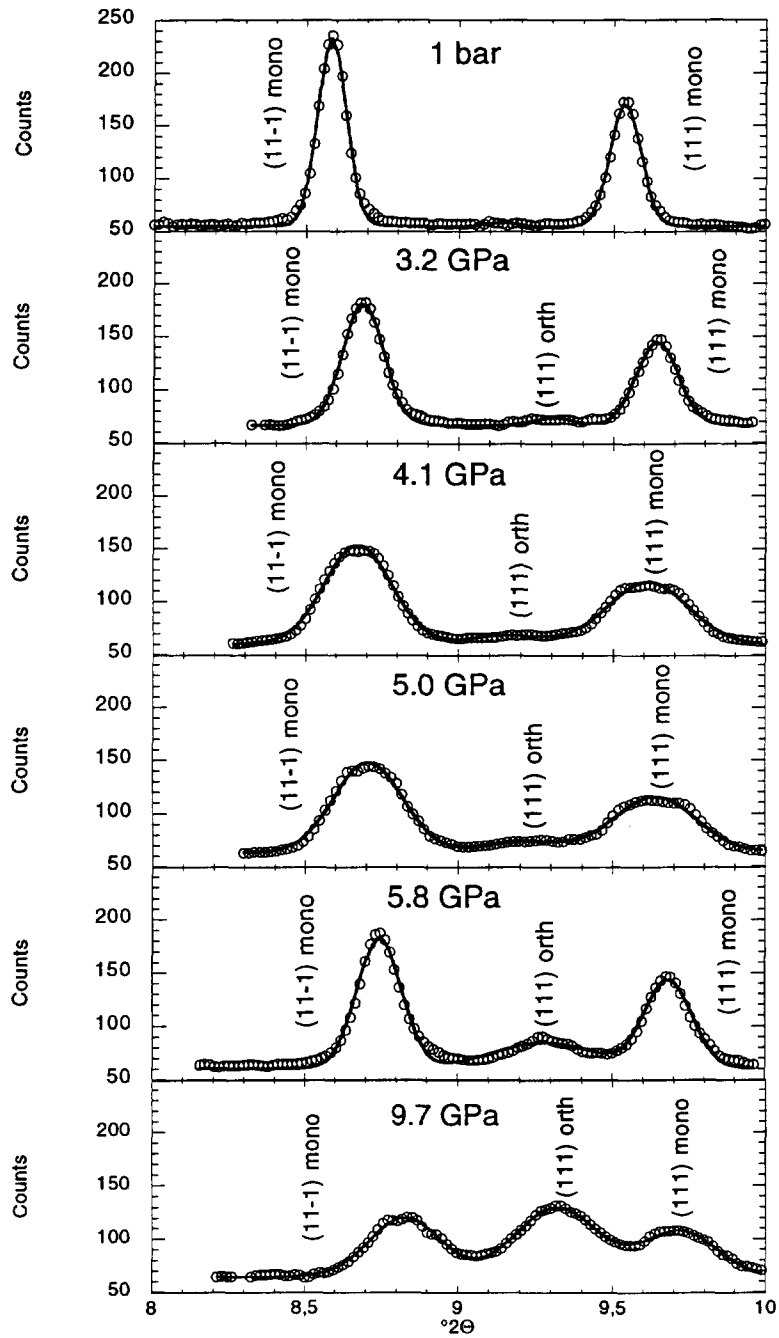

Figure 1. Angle-dispersive *in-situ* X-ray powder diffraction pattern of coarse-grained ZrO_2 at room temperature from 1 bar up to 10 GPa.

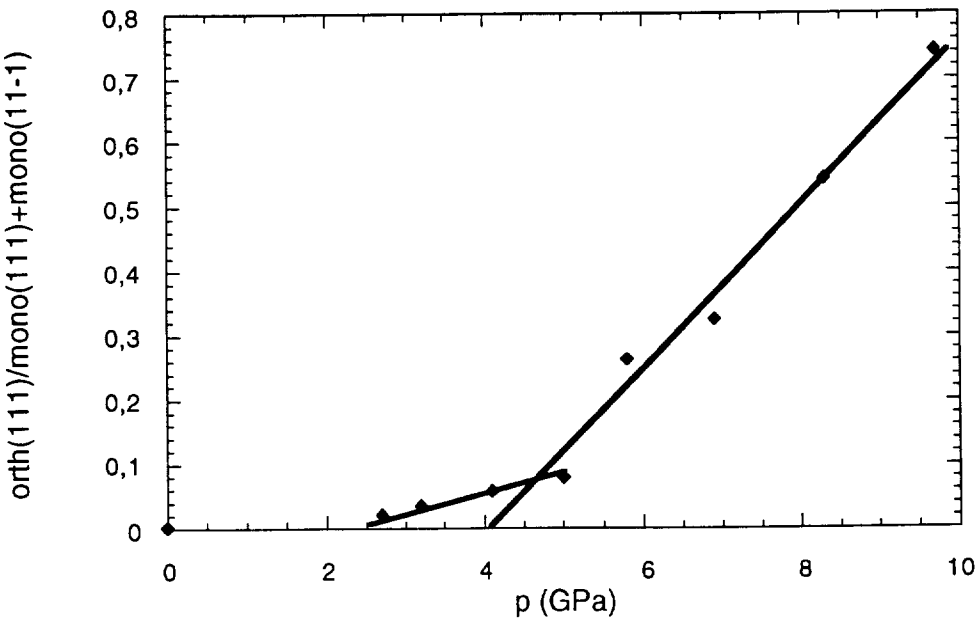

Figure 2. Ratio of the integral of the $(111)_{orth}$ peak and the sum of the $(111)_{mono}$ and $(11\text{-}1)_{mono}$ peaks for coarse-grained ZrO_2 from angle-dispersive data.

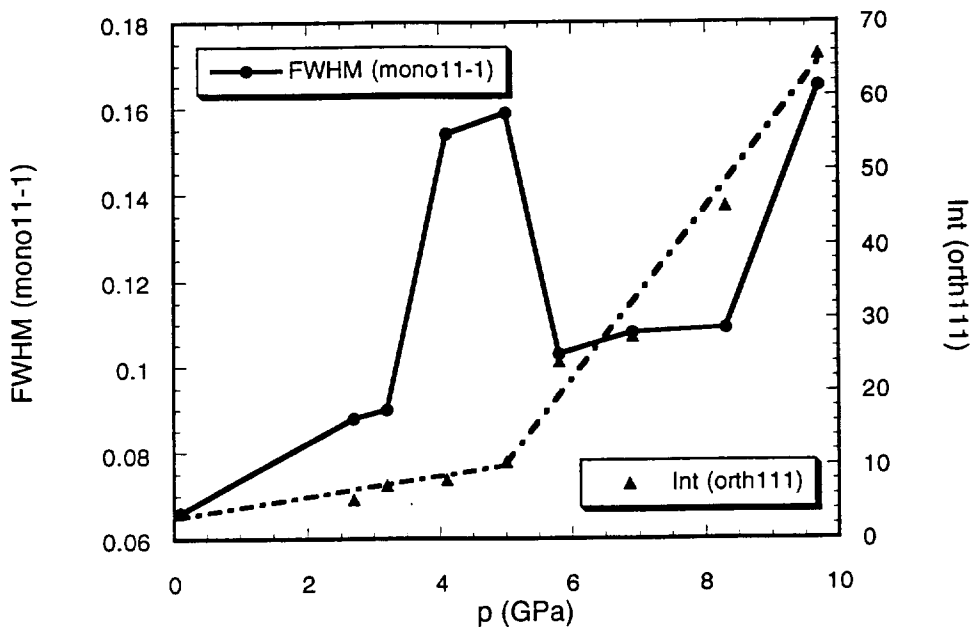

Figure 3. Correlation of line broadening of the $(11\text{-}1)_{mono}$ peak and the intensity of the $(111)_{orth}$ peak for coarse-grained ZrO_2 from angle-dispersive data.

Figure 2 shows the volume fraction of the high pressure phase calculated from the ratio of the integrated intensity of the $(111)_{orth}$ peak to the sum of the integrals of the $(11\text{-}1)_{mono}$ and $(111)_{mono}$ peaks as a function of pressure. In both angular and energy dispersive measurements we observe the beginning of a broad first-order phase transformation at about 2.5 to 3 GPa, which is still not fully completed at pressures as high as 10 GPa (Figure 2). This seems analogous to the pretransition regime observed for martensitic phase transitions at high temperature (13,19).

Line broadening is obvious for pressures between 4.1 GPa and 5.0 GPa. Broadening of the $(11\text{-}1)_{mono}$ peak reaches its maximum at about 5 GPa and is correlated with an increase of the $(111)_{orth}$ intensity up from 5 GPa (Figure 3). This indicates that between 3 and 5 GPa only a small number of particles transform, whereas the pressure increase is mostly compensated by large microstrain in the particles. Line positions increase in 2Θ during the rise of pressure corresponding to decreasing d-spacings upon compression (Figure 4). A second significant increase in the FWHM of the $(11\text{-}1)_{mono}$ peak in Figure 3 might be due to a second phase transition above approximately 10 GPa. Such a phase transition was described by Ohtaka *et al.* (20) between two different high pressure polymorphs (ortho I and ortho II).

Due to the large difference in density of the two phases and the volume discontinuity occuring at the thermal transition at ambient pressure, we also expect a sharp first order transition as a function of pressure. However, in our samples we find instead a very broad transition, as can be seen from the plot of the phase fraction as a function of pressure (Figure 2). This observation, together with the line broadening at intermediate pressure and the pretransition regime, leads us to conclude that the phase transformation is martensitic. Since martensitic transformations are athermal and displacive they are very fast and kinetics can be largely ignored. Line broadening is, then, a consequence of domain formation of the high pressure phase in the monoclinic matrix, producing local microscopic strain.

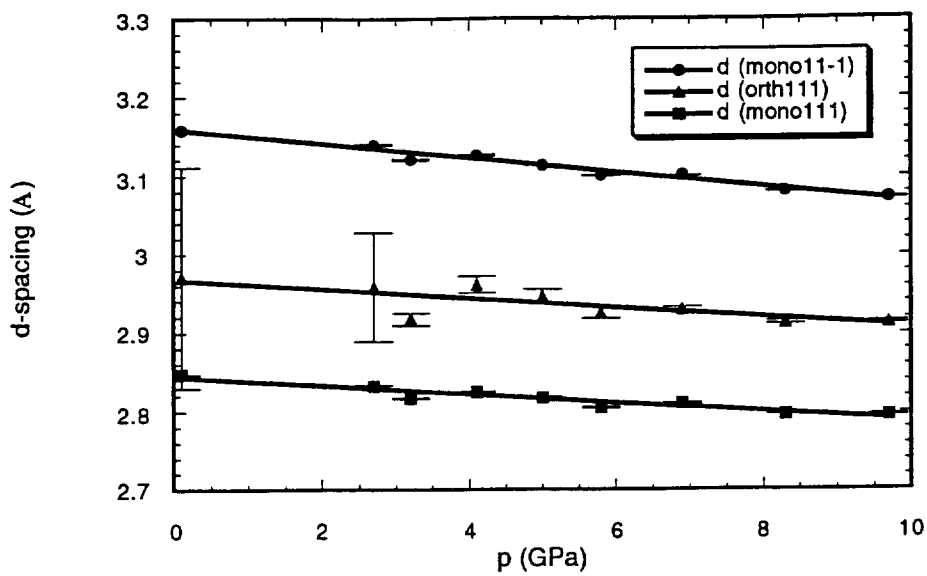

Figure 4. Decrease in d-spacings under pressure of the $(11\text{-}1)_{mono}$, $(111)_{orth}$ and $(111)_{mono}$ peaks for coarse-grained ZrO_2 from angle-dispersive data.

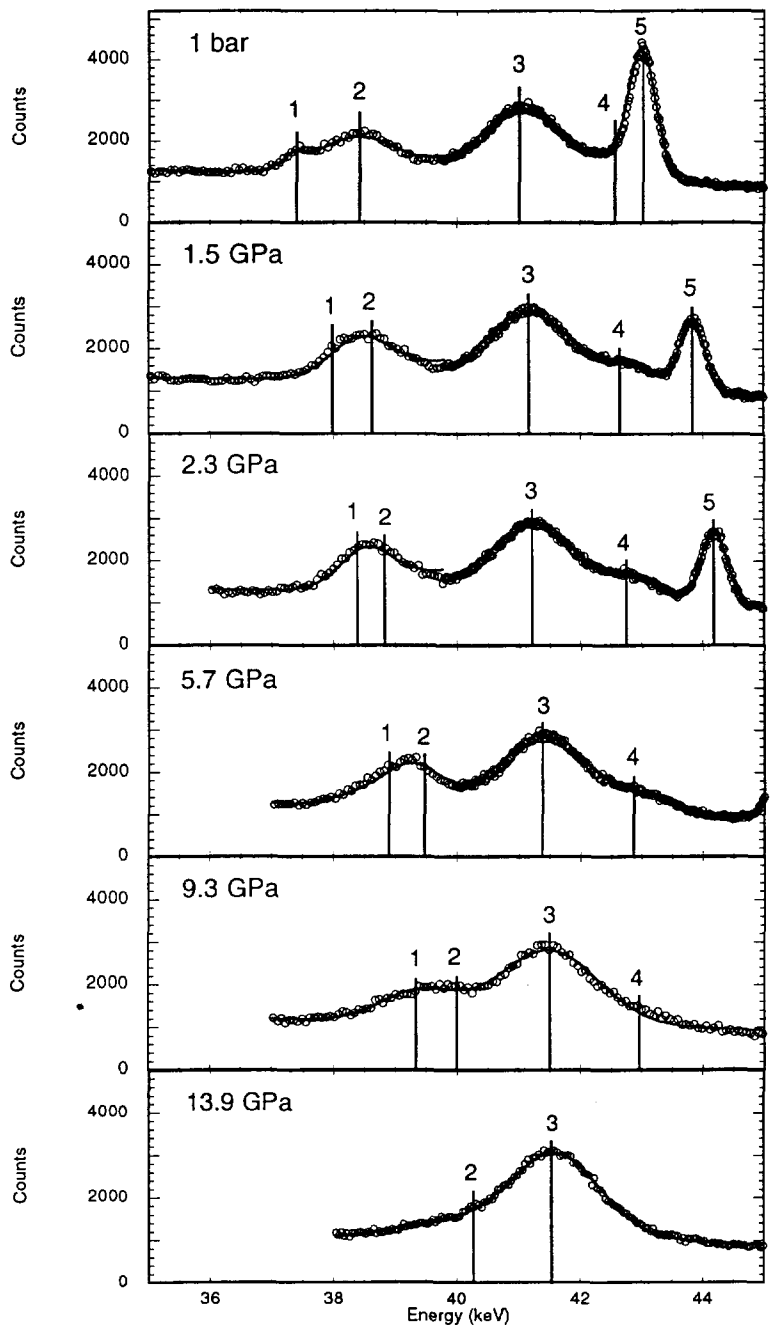

Figure 5. Energy-dispersive *in-situ* X-ray powder diffraction pattern of nanostructured ZrO_2 at room temperature for pressures ranging from 1 bar up to 14 GPa (1: $NaCl_{(100)}$, 2: monoclinic $ZrO_{2(11\text{-}1)}$, 3: tetr./orth. $ZrO_{2(111)}$, 4: monoclinic $ZrO_{2(111)}$, 5: $NaCl_{(111)}$).

(b) Nanocrystalline ZrO_2

Starting material for the high pressure experiment of n-ZrO_2 was a mixture of two polymorphs: about 40% monoclinic and 60% tetragonal. Rietveld analysis of the same powder confirmed the tetragonal structure at ambient pressure and temperature (8). The tetragonal phase is known to be stable at high temperature and high pressure (9,21). With increasing pressure n-ZrO_2 behaves similar to coarse-grained powder (Figure 5). The (111) peak intensity of the tetragonal phase in Figure 5 increases with increasing pressure, while the two peaks of the monoclinic phase decrease. Quantitative analysis is severely affected by the internal NaCl standard. A potential transformation from tetragonal to orthorhombic under high pressure cannot be observed in our experiments because of the large inherent line widths of the Bragg reflections due to the small particle size.

Since the majority of particles in our n-ZrO_2 are below the critical diameter for stabilization of the tetragonal phase (found experimentally by Garvie to be 30 nm), we interprete the phase mixture at ambient pressure in terms of an internal pressure which is larger than 2.5 GPa in about 60% of the particles (= relative amount of tetragonal phase in n-ZrO_2 powder, Figure 6). Increasing pressure would then transform the remaining monoclinic particles to a high pressure phase. The size dependent Gibbs free energy, $\Delta G(r)$, is given by (22):

$$\Delta G(r) = G_{tet}(r) - G_{mono}(r) = \frac{4}{3}\pi r^3 \Delta G_V + 4\pi r^2 \Delta\sigma \qquad [3]$$

where ΔG_V is the Gibbs free energy difference for the phase transition per unit volume and $\Delta\sigma$ is an estimate of the surface free energy difference. Assuming a critical radius where $G_{tet}(r)$ is equal to $G_{mono}(r)$ and therefore $\Delta G(r)$ becomes zero, we may calculate a critical radius, $r^* = 4$ nm, for the formation of the tetragonal phase simply by assuming isotropic, spherical particles:

$$r^* = -3 \cdot \frac{\Delta\sigma}{\Delta G_V} \qquad [4]$$

(using $\sigma_t = 0.77$ J /m^2, $\sigma_m = 1.13$ J /m^2 (2), $\Delta G_V = 2.46*10^8$ J/m^3 at 300 K (24) and an average molar volume of $2.092 \cdot 10^{-5}$ m^3/mol from the theoretical densities above). Another estimate for the critical radius is obtained from the integral particle size distribution function (Figure 6), where a fraction of 60 % is found at a particle radius of about 6 nm, which is in good agreement with the calculated critical radius from above.

With the modified equation [1], we estimate a surface stress of 5 N/m (using $\Delta p = 2.5$ GPa, $r = 4$ nm), which is larger than the surface free energy (of the order of 1 N/m). This inconsistency can be accounted for by considering equation [2], where the strain produces the second contribution to the surface energy (stress) with an isotropic contribution to the strain tensor $d\sigma/d\varepsilon$. Strain values could so far not be calculated from XRD data on n-ZrO_2.

Impurities or defects such as grain boundaries or large external surfaces affect phase transitions severely. Precursor phenomena, reduced latent heat, shifting and broadening of phase transitions have been found (25). Therefore, it is difficult to distinguish between a martensitic transition as in micrometer sized systems and size dependent effects, even if the particle size is well below the minimum [illegible] the martensitic domain formation.

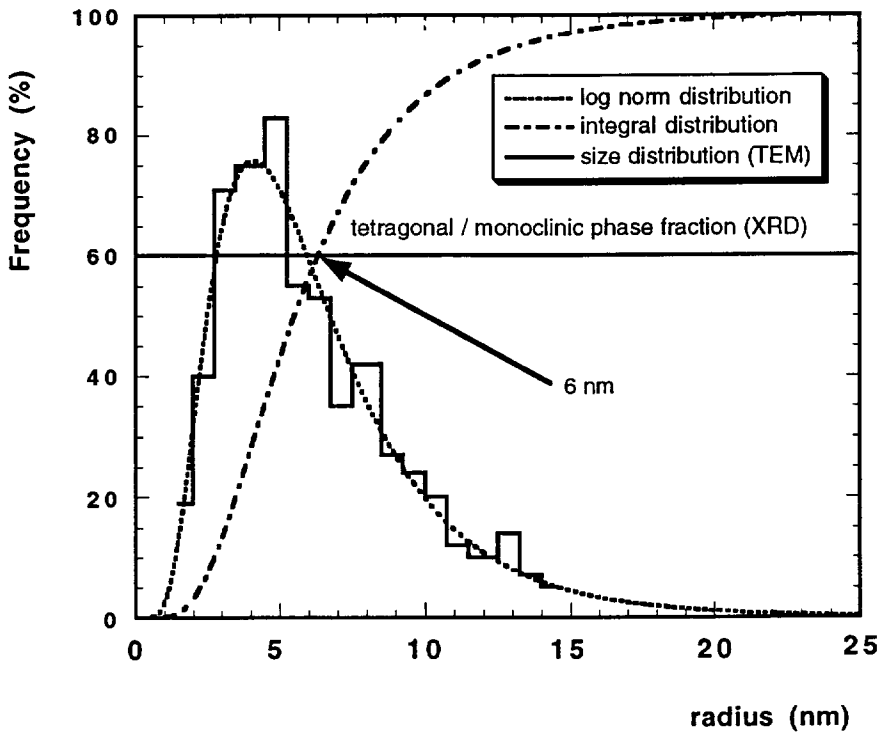

Figure 6. Particle size distribution of n-ZrO_2 powder from HRTEM micrographs fitted by a log normal distribution plotted together with the integral distribution.

More angle dispersive experiments on coarse grained as well as nanostructured ZrO_2 have to be performed with the aim of distinguishing between the tetragonal and the orthorhombic polymorphs. Furthermore, it is necessary to do *in-situ* high pressure experiments on monophase nanostructured material to investigate a shift in the critical pressure for the phase transition.

ACKNOWLEDGMENTS

The authors are grateful to R. Piltz and P. Hatton (the University of Edinburgh) for providing us with a diamond anvil cell and introducing us to the PLATYPUS program. Travel funding was provided by the LIP program of the European Union. We acknowledge the provision of synchrotron radiation and assistance from G. Bushnell-Wye at the beam line 9.1. by the Daresbury Laboratory/UK. We acknowledge the assistance of R. Rodewald during the HR-TEM analysis.

REFERENCES

1. O. Ruff and F. Ebert, Z. anorg. allgem. Chem. 180, 19 (1929).
2. R.C. Garvie, J. Phys. Chem. 69, 1238 (1965).

3. R.C. Garvie and P.S. Nicholson, J. Am. Ceram. Soc. 55, 304 (1972).
4. E. Bernstein, M.G. Blanchin, R. Ravelle-Chapius, and J. Rodriguez-Carvajal, J. Mat. Sci. 27, 6519 (1992).
5. G. Skandan, C.M. Foster, H. Frase, M.N. Ali, J.C. Parker, and H. Hahn, Nanostruct. Mater. 1, 313 (1992).
6. W. Chang, F. Cosandey, and H. Hahn, Nanostruct. Mater. 2, 29 (1993).
7. D. Schroeer and R.C. Nininger, Phys. Rev. Lett. 15, 633 (1967).
8. R. Nitsche, W.W. Schmahl, and H. Hahn, in preparation.
9. J.M. Leger, P.E. Tomaszewski, A. Atouf, and A.S. Pereira, Phys. Rev. B 47, 14075 (1993)
10. J.S. Vermaak, C.W. Mays, and D. Kuhlmann-Wilsdorf, Surf. Science 12, 128 (1968).
11. C.W. Mays, J.S. Vermaak, and D. Kuhlmann-Wilsdorf, Surf. Science 12, 134 (1968).
12. R.C. Camarata and K. Sieradski, Phys. Rev. Lett. 17, 2005 (1989).
13. H. Boysen, F. Frey, and T. Vogt, Acta Cryst. B47, 881 (1991).
14. G.M. Wolten, J. Am. Ceram. Soc. 46, 419 (1963).
15. H. Hahn, J.A. Eastman, and R.W. Siegel, Ceramic Transactions 1b, Ceramic Powder Science, 1115 (1988).
16. R.O. Piltz, M.I. McMahon, J. Crain, P.D. Hatton, R.J. Nelmes, R.J. Cernik, and G. Bushnell-Wye, Rev. Sci. Instr. 63, 700 (1992).
17. G.J. Piermarini and S. Block, Rev. Sci. Instr. 46, 973 (1975).
18. D.L. Decker, J. Appl. Phys. 42, 3239 (1971).
19. F. Frey, H. Boysen, and T. Vogt, Acta Cryst. B46, 724 (1990).
20. O. Othaka, T. Wyamanaka, S. Kume, E. Ito, and A. Navrotsky, J. Am. Ceram. Soc. 74, 505 (1991).
21. P. Li, I-Wei Chen, and J.E. Penner-Hahn, Phys. Rev. B 48, 10063 (1993).
22. W.D. Kingery, H.K. Bowe, and P.R. Uhlmann, *Introduction to Ceramics*, Wiley, New York (1976).
23. R.C. Garvie, J. Phys. Chem. 82, 218 (1978)
24. E.D. Whitney, J. Am. Ceram. Soc. 45, 612 (1962).
25. K. Binder, "Statistical Theories of Phase Transitions," in *Materials Science and Technology* , eds. R.W. Cahn, P. Haasen, and E.J. Kramer, Vol. 5, VCH, Weinheim, p. 144 (1991).